**WOOD RESEARCH** doi.org/10.37763/wr.1336-4561/67.1.6375
**e-ISSN 2729-8906**
**67(1): 2022 63-75 pp.**

# INFLUENCE OF SIZE EFFECT ON THE BEARING CAPACITY OF THE AXIALLY COMPRESSED COMPONENTS OF CORN STRAW INTEGRATED MATERIAL AND ITS CALCULATION METHOD

XUE FENG, BOXIN WANG
JILIN UNIVERSITY
CHINA

YONGMEI QIAN, WEI TIAN
JILIN JIANZHU UNIVERSITY
CHINA

(RECEIVED MAY 2021)

## ABSTRACT

Our paper proposed a new type of environmentally friendly biomass material, corn straw integrated material (CSIM). In this paper, the ultimate bearing capacity of the axially compressed components under parallel, vertical and combined texture-integrated methods are compared and analyzed through the experimental research. The influence of size effect on the bearing capacity of the axially compressed components of the CSIM is determined, and the calculation method of the bearing capacity of the axially compressed components under vertical texture-integrated method is proposed. Results showed that the slenderness ratio of 35 was the dividing point between the strength and instability failures of the CSIM axially compressed component, and the calculated value of the revised bearing capacity calculation method agreed with the test value. The result is very close to the American National design specification for wood construction (ANSI/AF&PA NDS, 2005).

KEYWORDS: Corn straw integrated material, size effect, cross-section aspect ratio, slenderness ratio, axial compression.

## INTRODUCTION

In the past, traditional biomass building materials rely on wood. However, excessive deforestation, lack of forest resources, and characteristics of flammable, perishable, and insect-eaten wood severely restrict the application and development of biomass building materials (Lazar and Chithra 2020). The corn straw integrated material (CSIM) is a new type of

biomass high-strength composite material produced through a series of processes, such as reorganization and integration of corn straw fiber raw materials. According to the different horizontal and vertical textures, the corn straw restructured plank can be made into parallel, vertical, and combined texture-integrated materials. The corn straw restructured plank has excellent characteristics, such as high strength, high hardness, insect resistance, moisture resistance, corrosion resistance, high fire resistance, and good compression mechanical properties (Qian et al. 2019a).

Straws as a building material first appeared in the 19th century when the residents of Nebraska, USA used straw bricks made of straw stalks to build brick walls to support their roofs (Kammoun and Trabelsi 2020). At the beginning of the 20th century, the United Kingdom, Poland, and other countries mastered the production technology of straw wood-based panels (Marques et al. 2020, Owodunni et al. 2020). At present, straw wood-based panel processing plants led by the United States have spread in more than 20 countries around the world (Mehrmashhadi et al. 2019), and the development and utilization of straw materials are well developed. The research of stem-based biomass building materials in China particularly in the research of stem-based and straw panels began in the 1980s (Tu 2004, Liuzzi et al. 2020, Aladejana et al. 2020, Koh and Kraniotis 2020, Chinh et al. 2020). In 2006, the first continuous production line of straw plank established by China Yantai Wanhua Group was officially put into production (Liu et al. 2019), which put the research on straw building materials go further.

In recent years, integrated wood (Wechsler and Hiziroglu 2007, Leggate et al. 2020), integrated bamboo (Li et al. 2019, Wei et al. 2020), and straw-based integrated wood (Soroushian et al. 2004) have received increasing research and applications, thereby promoting the development of biomass building materials. At present, domestic and foreign straw-based biomass building materials are mostly made of wood-based panels, bamboo–wood (metal/concrete) composite materials, and reinforced cement-based materials (Zhao et al. 2019, Hu et al. 2020, Sun et al. 2020). The stem-based panel is a man-made synthetic plank made by hot pressing and other processes after the stalk is processed into particles. The stem-based panel cannot be used as a building structural material during use and is mostly used in carriage floor and as furniture material and decoration (Yang et al. 2020, Qian et al. 2019b, Wang et al. 2019, Qi et al. 2019, Titirla et al. 2020, Xie et al. 2020). According to the preliminary experimental research of the research group, it is different from the processing technology and application scope of the stem-based panel's materials currently on the market. The integrated material processed and produced from corn straw intact fiber makes up for the shortcomings of existing materials and can be used in traditional home decoration and as building structural materials.

Therefore, this paper adopts the CSIM as a new type of biomass building structural material and studies the equal-scale axially compressed components of the CSIM by using three integration methods (i.e. parallel, vertical, and combined texture-integrated). By comparing the ultimate bearing capacity of the axially compressed components with different size parameters, the influence of factors, such as cross-section aspect and slenderness ratios, on the bearing capacity of axially compressed components is analyzed. The theoretical value of the bearing capacity in the specification is compared with the experimental value, and the calculation method of the bearing capacity of the axially compressed component with

the vertical texture-integrated is proposed. The calculation method provides theoretical support for the application of CSIM in building structures and promotes the effective use of corn straws as agricultural waste and environmental protection in the building materials industry.

## MATERIAL AND METHODS

Corn straw integrated material (CSIM) is composed of corn straw restructured planks, which are processed and produced by sizing and pressing with a factory cold press. Corn straw recombination material, is a new type of high-strength composite material that is formed by layer-by-layer overlaying and sizing and pressing of corn straw fibers (Qian et al. 2019a,b, Tian et al. 2020), as shown in Fig. 1.

According to the different transverse and longitudinal textures of the cross-section of the recombination material, recombination material were cut into planks along the X- and Y-directions to obtain the parallel texture plank and the vertical texture plank of the corn straw recombination material. The planks with different textures were sized, pressed and integrated to obtain the corn straw parallel texture, vertical texture or combined texture components.

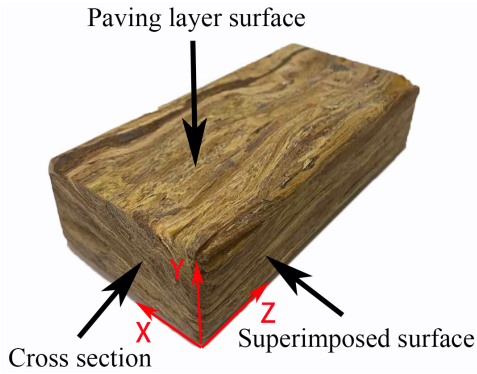


*Fig. 1: Corn straw recombination material.*

Considering that different integration methods have different mechanical properties, the axial compression test was carried out on the components of three integration methods to study the influence of different size parameters on the bearing capacity of the axial compression components of the CSIM.

In this paper, the JAY-10000KN microcomputer-controlled electrohydraulic servo pressure testing machine was used to carry out the uniform speed loading test. Test was terminated when the test specimen failed. The axially compressed components of the CSIM were divided into three groups, i.e., P, V, and C, which represented parallel, vertical, and combined texture-integrated methods, respectively. The components had cross-sectional dimensions of 150 × 150 mm and 150 × 180 mm and heights of 1000 mm and 1800 mm. The thickness of the integrated plank was 30 mm, and a total of 12 integrated material axial compression column components were designed. The calculation of Slenderness ratio $\lambda$ refers to the American *National design specification for wood construction* (ANSI/AF&PA NDS, 2005).

The physical specimens are shown in Fig. 2. The arrangement of measuring points is shown in Fig. 3, and the specific design parameters of the component are presented in Tab. 1.

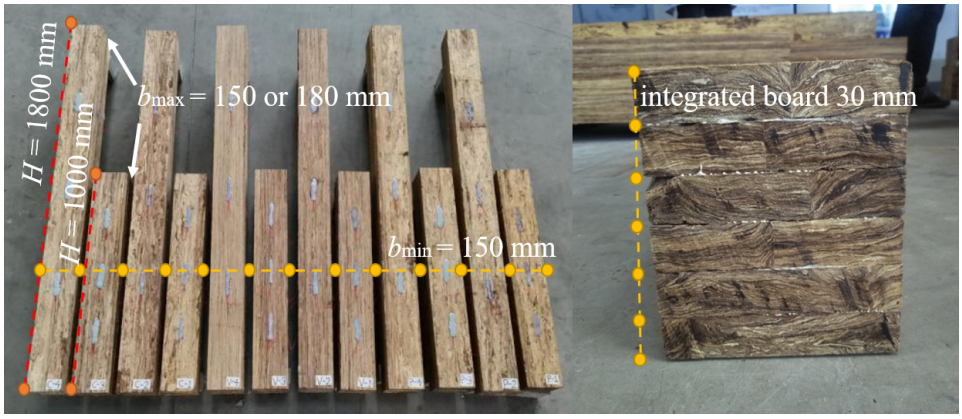


*Fig. 2: CSIM specimens.*

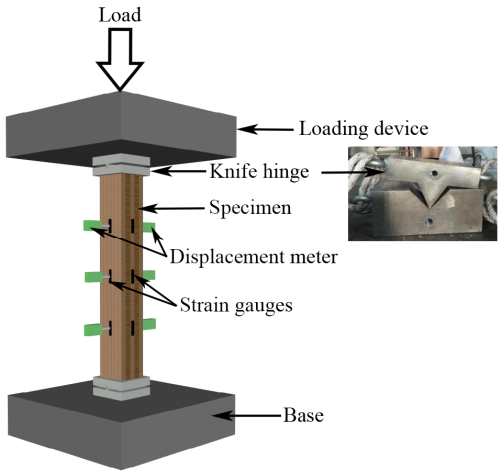


*Fig. 3: Location of measuring points.*

*Tab. 1: Design parameters of the CSIM.*

| Integrated texture | Specimen number | Number | Sectional dimension, $b_{max}$ (mm) × $b_{min}$ (mm) | Height (mm) | Cross-section aspect ratio, $b_{max}/b_{min}$ | Slenderness ratio, $\lambda$ |
|---|---|---|---|---|---|---|
| Parallel texture integration | P-1 | 1 | 150 × 150 | 1000 | 1.0 | 23.09 |
| | P-2 | 1 | 150 × 150 | 1800 | 1.0 | 41.57 |
| | P-3 | 1 | 150 × 180 | 1000 | 1.2 | 19.24 |
| | P-4 | 1 | 150 × 180 | 1800 | 1.2 | 34.64 |
| Vertical texture integration | V-1 | 1 | 150 × 150 | 1000 | 1.0 | 23.09 |
| | V-2 | 1 | 150 × 150 | 1800 | 1.0 | 41.57 |
| | V-3 | 1 | 150 × 180 | 1000 | 1.2 | 19.24 |
| | V-4 | 1 | 150 × 180 | 1800 | 1.2 | 34.64 |
| Combined texture integration | C-1 | 1 | 150 × 150 | 1000 | 1.0 | 23.09 |
| | C-2 | 1 | 150 × 150 | 1800 | 1.0 | 41.57 |
| | C-3 | 1 | 150 × 180 | 1000 | 1.2 | 19.24 |
| | C-4 | 1 | 150 × 180 | 1800 | 1.2 | 34.64 |

## RESULTS AND DISCUSSION

The failure traits of the CSIM are strength and instability failures. The strength failure is divided into split and end partial pressure failures. The instability failure is an overall buckling failure, and the failure mode of the CSIM is similar to that of steel–wood (bamboo) composites under axial compression (Razavian et al. 2020, Zhang et al. 2020). All components are divided into four groups. Group 1 contains P-1, V-1, and C-1. Group 2 includes P-2, V-2, and C-2. Group 3 includes P-3, V-3, and C-3. Group 4 contains P-4, V-4, and C-4. The following is an analysis of the effect of size parameters on the bearing capacity of the axially compressed components of CSIM under different integration methods through the cross-sectional aspect and slenderness ratios, and proposes the calculation method for the bearing capacity of vertical texture-integrated axial compression components.

Plotted the midpoint cross-sectional stress–strain relationship curve of all components of the CSIM, as shown in Fig. 4.

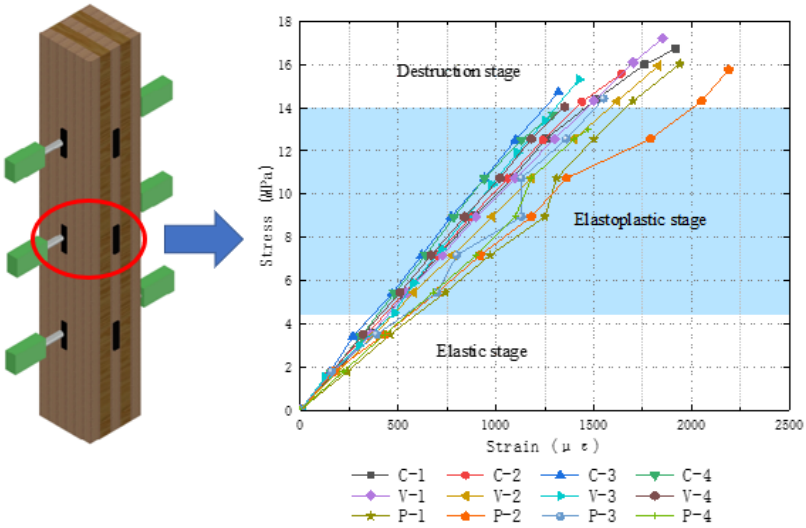


*Fig. 4: Stress–strain curve of all components.*

Research results show that the strain increases with stress during the whole loading process of axially compressed components. In the initial stage of test loading, the strain of the component increases linearly with stress. In the elastic stage, the slope of the stress–strain curve is basically the same, and the developed stress–strain relationship that the component under axial compression is regular. When the test enters the late stage of elastoplasticity, the slope of the stress–strain curve of each specimen gradually slows down. In the whole process, no evident yield platform and a descending section for each integrated axial compression component are observed. When the bearing capacity reaches the ultimate load, the material suddenly fails without evident plastic deformation. When the test force is relieved, the axial deformation of each component is generally restored to a straight state, indicating that although the axial compression component of the CSIM has a certain elastoplasticity when broken, CSIM is generally brittle. Under the condition of same section size, a high slenderness ratio of the

component results in low stress. At the same column height, a small section size of the component increases the stress.

**Influence of cross-section aspect ratio on the bearing capacity**

Among the three components under different integration methods, components with different cross-sectional aspect ratios and same integration method and height are selected for comparison. Figs. 5a-c are the load–axial displacement comparison curves of groups 1 and 3 under parallel, vertical, and combined texture-integrated methods. Figs. 5d-f are the load–axial displacement comparison curves of groups 2 and 4 under parallel, vertical, and combined texture-integrated methods.

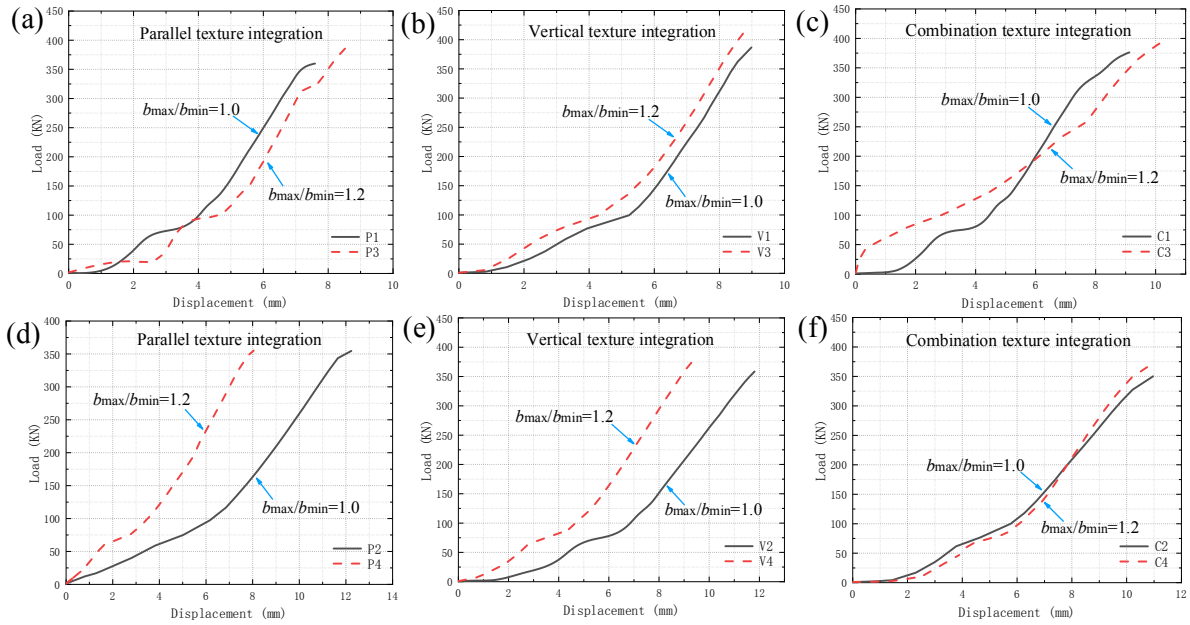


*Fig. 5: Load–axial displacement curves of components with different cross-section aspect ratios. Groups 1 and 3 under parallel (a), vertical (b), and combined (c) texture-integrated methods. Groups 2 and 4 under parallel (d), vertical (e), and combined (f) texture-integrated methods.*

Fig. 5 shows that with increasing cross-section aspect ratio, increased ultimate load of the component and decreased axial displacement are observed. Compared with those of components under parallel and combined texture-integrated methods, the curve growth trend of components under the vertical texture-integrated is more regular under the same load. In the whole process of loading, the components exhibit mechanical properties, and a large cross-section aspect ratio results in strong ultimate load-carrying capacity. The large cross-section aspect ratio of the individual components under the parallel texture-integrated results in low ultimate load-bearing capacity. This phenomenon occurred when the parallel texture-integrated plank is subjected to axial pressure, the cracks generated follow the longitudinal texture of the component, and the internal bonding capacity of the material is weakened. When the crack develops to a certain extent, the component loses its load-bearing

capacity and reaches destruction, and the vertical texture-integrated plank limits the development of the crack under the action of the axial pressure, thereby improving the load-bearing capacity of the component.

**Influence of slenderness ratio on the bearing capacity**

The components with different slenderness ratios under the three integration methods are compared. Figs. 6a-c plot the load–axial displacement comparison curves of the components with different slenderness ratios under the parallel, vertical, and combined texture-integrated methods, resp.

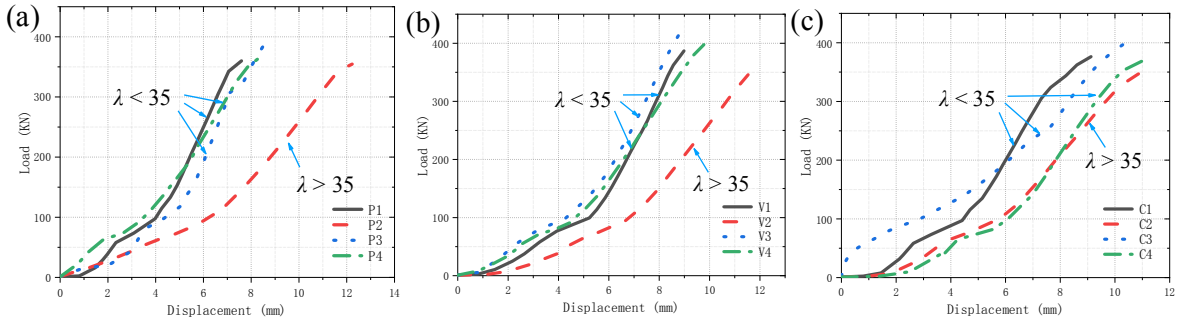


*Fig. 6: Load–axial displacement curves of components with different slenderness ratios under parallel (a), vertical (b), and combined (c) texture-integrated methods.*

Fig. 6 shows that as the slenderness ratio increases, the bearing capacity of the axially compressed components of each integration method is significantly reduced. From the perspective of the trend of displacement with load, a high slenderness ratio of the component results in high displacement change. Under the same load, the displacement of the component under the parallel texture-integrated is the largest followed by that under the combined texture-integrated. The component under the vertical texture-integrated has the smallest displacement. The load–displacement relationship increases linearly during the entire process from the beginning of loading to the ultimate load. The load–axial displacement curve shows that the axial displacement value of the component with $\lambda > 35$ is greater than that of the component with $\lambda < 35$. The curve trend of the vertical texture-integrated component is regular, and the load change under the axial pressure has good reliability and predictability. When the component is subjected to axial pressure, a small slenderness ratio results in strong bearing capacity.

The ultimate load–slenderness ratio comparison curve of different integration methods is drawn and shown in Fig. 7. The above data show that among the three integration methods of the CSIM, the vertical texture-integrated provides the highest ultimate bearing capacity followed by the combined and parallel texture-integrated methods. The trend of the ultimate load–slenderness ratio curve of the three integrated axially compressed components is the same. With increasing slenderness ratio, the ultimate load of the axially compressed components of each integration method gradually decreases. Given that the *Technical code of glued laminated timber structures* (GBT50708, 2012) and the *National design specification for wood*

*construction* (ANSI/AF&PA NDS, 2005) require that the slenderness ratio for solid columns shall not exceed 50, when the slenderness ratio is higher than 40, the bearing capacity of the component decreases remarkable. Combined with the test results in this paper, the study shows that when $\lambda > 35$, the ultimate bearing capacity of the axially compressed components under various integration methods of CSIM is significantly reduced, and the axial displacement is significantly increased. It indicates that this is the dividing point between the strength failure and the instability failure of the axially compressed component. When $\lambda < 35$, the component has strength failure. When $35 < \lambda < 40$, the component has strength and instability failures, and when $\lambda > 40$, the component has the instability failure.

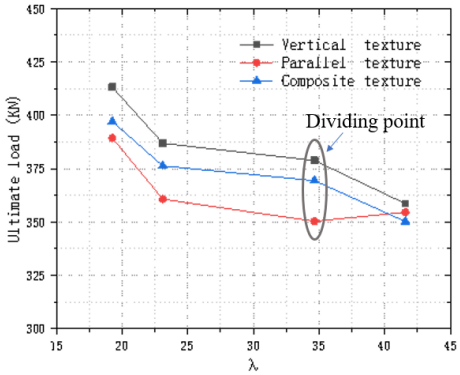


*Fig. 7: Load–slenderness ratio comparison curve of components under different integration methods.*

In summary, the cross-sectional aspect and slenderness ratios as different size parameters of the components have a higher effect on the compressive bearing capacity of the CSIM. The cross-sectional aspect ratio determines the bearing capacity of the component, and the slenderness ratio determines the difference in the failure traits of the component. However, increasing the cross-section aspect ratio reduces the slenderness ratio of the component, affects the damage traits of the component, and increases the engineering cost. Therefore, the rationality of the cross-section aspect and the slenderness ratios should be fully considered in the component design.

**Calculation method of the bearing capacity of the axially compressed component under the vertical texture-integrated**

Based on the above research, under the action of axial compression, the vertical texture-integrated method has the highest bearing capacity among the three integration methods of CSIM. This finding shows that when using an axially compressed component, the optimal integration method is the vertical texture-integrated method. The calculation method of the bearing capacity of the axially compressed component under the vertical texture-integrated is analyzed below. The bearing capacity test results of axially compressed components with different slenderness ratios are compared with that in the American *National design specification for wood construction* (ANSI/AF&PA NDS, 2005). The slenderness ratio–ultimate load comparison curve of the axially compressed components under the vertical

texture-integrated is shown in Fig. 8. Figs. 11a,b show specimens with sectional dimensions of 150 × 150 mm and 150 × 180 mm.

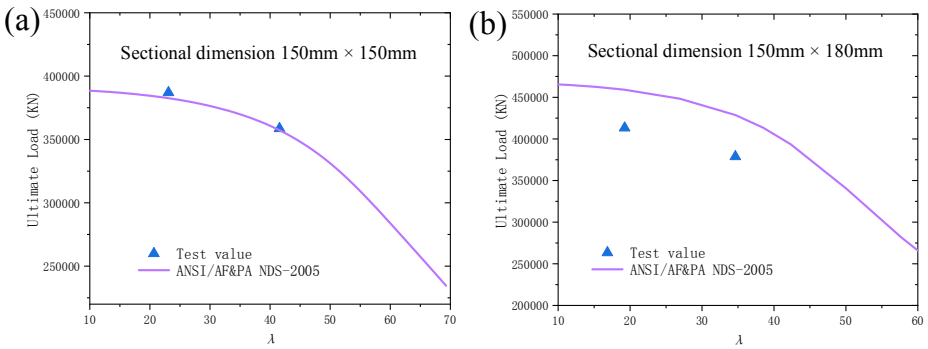


*Fig. 8: Load–slenderness ratio comparison curve of the axially compressed component under the vertical texture-integrated. Sectional dimensions 150 × 150 mm (a), 150 × 180 mm (b).*

Fig. 8a shows that for components with equal cross-section sides, test results are close to the calculated results of the American *National design specification for wood construction*. This finding shows that the American *National design specification for wood construction* applies to the calculation of the ultimate bearing capacity of the vertical texture-integrated axial compression component of the CSIM. For components with unequal cross-section side lengths, the actual test results are quite different from the specification calculated values, and the effective side lengths ($b_c$) in the specification should be introduced to modify the formula (Fig. 8b). The calculation formula of the vertical texture-integrated axial compression bearing capacity of CSIM is established:

$$N = \varphi b_c^{\,2} f_c \tag{1}$$

where: $N$ - axial compression design value for the vertical texture-integrated material (N), $\varphi$ - stability coefficient, $b_c$ - effective side lengths (mm), $f_c$ - compressive strength design value parallel to the grain of vertical texture-integrated material ($N \cdot mm^{-2}$), $f_c$ = 17.32 MPa.

The CSIM, a reorganized integrated material, is different from wood in terms of specifications, and the calculated area of the cross-section of the compression component is different from that of ordinary wood. Therefore, when calculating the bearing capacity of axially compressed components, $b_c$ is introduced in this article to correct the calculated area of the axial compression component cross-section in the calculation formula of bearing capacity. The calculation coefficient of the support condition in the original $b_c$ calculation formula is removed to avoid repeated calculations, and the calculation is adjusted to the formula:

$$b_c = b_{\min} + 0.15(b_{\max} - b_{\min})(b_{\min} / b_{\max}) \tag{2}$$

where: $b_{\max}$ - maximum dimension for that face of the column (mm), and $b_{\min}$ - minimum dimension for that face of the column (mm).

The stability coefficient ($\varphi$) in Eq. 1 is calculated in accordance with $\varphi$ of axially compressed components in the American National design specification for wood construction:

$$\varphi = \frac{1+(f_{cE}/f_c)}{2c} - \sqrt{\left[\frac{1+(f_{cE}/f_c)}{2c}\right]^2 - \frac{f_{cE}/f_c}{c}} \quad (3)$$

where:

$$f_{cE} = \frac{0.822 E_{\min}'}{(l_0/b_c)^2} \quad (4)$$

and

$$E_{\min}' = E[1-1.645COV_E](1.05)/1.66 \quad (5)$$

where: $f_{cE}$ - critical buckling strength design value for compressive parallel to grain (N·mm$^{-2}$), $c$ = 0.9 for bending coefficient for glued laminated timber, $E_{min}'$ - reference and adjusted moduli of elasticity for stability calculations (N·mm$^{-2}$), $l_0$ - effective length (mm), $E$ - elastic modulus (N·mm$^{-2}$), $E$ = 11053 MPa, $COV_E$ = 0.1 for the coefficient of variation of elastic modulus.

The calculation curves of the bearing capacity before and after correction with the test values are compared. Figs. 9a,b plot the slenderness ratio–ultimate load comparison curves of the test value, specification value, and the value calculated using the modified formula of the specimen with the cross-section size of 150 × 150 mm and 150 × 180 mm.

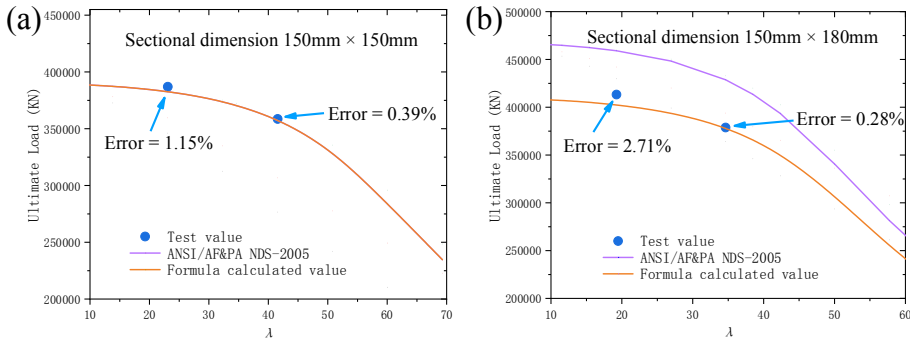


*Fig. 9: Load–slenderness ratio comparison curve of the axially compressed component under the vertical texture*-integrated*: Sectional dimension 150 × 150 mm (a), Sectional dimensions 150 × 180 mm (b).*

Figs. 9a,b show that the average error between the value calculated using the modified formula and the measured ultimate load in the test is 1.13%. The data are in good agreement, indicating that this calculation method can effectively predict the ultimate bearing capacity of vertical texture-integrated axial compression components. The above calculation method can be used as a theoretical basis for the study of the ultimate bearing capacity of the axial compressed components of CSIM under the vertical texture-integrated.

## CONCLUSIONS

This paper studies the influence of size effect on the bearing capacity of the axially compressed components of CSIM and provides a reference for the promotion and design of new biomass building structural materials. The following conclusions can be drawn from this study: *(1)* On the basis of the calculation method of the bearing capacity of axially compressed components in the American National design specification for wood construction, $b_c$ is introduced and modified to improve the formula. A calculation method for the axial compression bearing capacity of the component of the CSIM under the vertical texture-integrated is proposed. The theoretical calculation value obtained by this calculation method agrees with the experimental value, which can effectively predict the ultimate bearing capacity of the axially compressed component under the vertical texture-integrated. *(2)* The failure traits of the axially compressed components of the CSIM are divided into strength and instability failures. $\lambda = 35$ is the cutoff point between the strength and instability failures of the axially compressed components. When $\lambda < 35$, the component has strength failure, when $35 < \lambda < 40$, the component has strength and instability failures, and when $\lambda > 40$, the component has instability failure. *(3)* For the axially compressed components of CSIM, a large slenderness ratio results in small bearing capacity under the condition of the same cross-sectional aspect ratio. At the same column height, as the cross-sectional aspect ratio increases, decreased slenderness ratio, increased bearing capacity, and increased damage phenomenon are observed. *(4)* From the perspective of integrated texture, the parallel texture-integrated plank reduces the bearing capacity of the component when subjected to axial pressure, whereas the vertical texture-integrated plank can improve the overall strength of the component, and the vertical texture-integrated provides higher material stability after failure than the two other integration method.

## ACKNOWLEDGMENTS

This research work was financially supported by the Key Science and Technology Projects in Jilin Province, China (Grant No. 20180201066SF). The authors have no conflict of interest to declare.

## REFERENCES

1. Aladejana, J.T., Wu, Z., Fan, M., Xie, Y., 2020: Key advances in development of straw fibre bio-composite boards: An overview. Materials Research Express 7(1): 1-19.
2. Chinh Van, N., Mangat, P.S., 2020: Properties of rice straw reinforced alkali activated cementitious composites. Construction and Building Materials 261(2): 120536.
3. Hu, Q., Gao, Y., Meng, X., Diao, Y., 2020: Axial compression of steel-timber composite column consisting of H-shaped steel and glulam. Engineering Structures 216: 110561.
4. Kammoun, Z., Trabelsi, A., 2020: A high-strength lightweight concrete mace using straw. Magazine of Concrete Research 72(9): 460-470.

5. Koh, C.H., Kraniotis, D., 2020: A review of material properties and performance of straw bale as building material. Construction and Building Materials 259: 120385.
6. Lazar, N., Chithra, K., 2020: A comprehensive literature review on development of building sustainability assessment systems. Journal of Building Engineering 32: 101450.
7. Leggate, W., McGavin, R.L., Miao, C., Outhwaite, A., Chandra, K., Dorries, J., Kumar, C., Knackstedt, M., 2020: The influence of mechanical surface preparation methods on southern pine and spotted gum wood properties: Wettability and Permeability. Bioresources 15(4): 8554-8576.
8. Li, H.T., Liu, R., Lorenzo, R., Wu, G., Wang, L.B., 2019: Eccentric compression properties of laminated bamboo columns with different slenderness ratios. Proceedings of the Institution of Civil Engineers: Structures and Buildings 172(5): 314-326.
9. Liu, H.G., Luo, B., Shen, S.J., Li, L., 2019: Review of research and development of straw building materials. Forestry Machinery & Woodworking Equipment 47(05): 4-12.
10. Liuzzi, S., Rubino, C., Martellotta, F., Stefanizzi, P., Casavola, C., Pappalettera, G., 2020: Characterization of biomass-based materials for building applications: The case of straw and olive tree waste. Industrial Crops and Products 147: 112229.
11. Marques, B., Tadeu, A., Almeida, J., Antonio, J., de Brito, J., 2020: Characterisation of sustainable building walls made from rice straw bales. Journal of Building Engineering 28: 101041.
12. Mehrmashhadi, J., Chen, Z.G., Zhao, J.M., Bobaru, F., 2019: A stochastically homogenized peridynamic model for intraply fracture in fiber-reinforced composites. Composites Science and Technology 182: 107770.
13. Owodunni, A.A., Lamaming, J., Hashim, R., Taiwo, O.F.A., Hussin, M.H., Mohamad Kassim, M.H., Bustami, Y., Sulaiman, O., Amini, M.H.M., Hiziroglu, S., 2020: Adhesive application on particleboard from natural fibers: A review. Polymer Composites 41(11): 4448-4460.
14. Qi, Y., Xie, L., Bai, Y., Liu, W., Fang, H., 2019: Axial compression behaviours of pultruded GFRP-Wood Composite Columns. Sensors 19(4): 755.
15. Qian, Y.M., Feng, X., Tian, W., Liu, Z.P., 2019a: Experimental research on compressive performance parameters of new type corn straw. Industrial Construction 49(08): 163-166.
16. Qian, Y.M., Feng, X., Tian, W., 2019b: Preliminary study on mechanical properties of corn straw recombinant glulam. Building Structure 49(S1): 273-275.
17. Razavian, L., Naghipour, M., Shariati, M., Safa, M., 2020: Experimental study of the behavior of composite timber columns confined with hollow rectangular steel sections under compression. Structural engineering and mechanics 74(1): 145-156.
18. Soroushian, P., Aouadi, F., Chowdhury, H., Nossoni, A., Sarwar, G., 2004: Cement-bonded straw board subjected to accelerated processing. Cement & Concrete Composites 26(7): 797-802.
19. Sun, X., He, M., Li, Z., 2020: Novel engineered wood and bamboo composites for structural applications: State-of-art of manufacturing technology and mechanical performance evaluation. Construction & Building Materials 249: 118751.

20. Titirla, M.D., Ferrier, E., Michel, L., 2020: On the mechanical behaviour of innovative moment connections between composite floor panels and glulam columns. International Journal of Architectural Heritage15(2): 321-333.
21. Tian, W., Wang, Y.M., Qian, Y.M., Wang, R.Z., 2020: Finite element modeling and analysis of tensile strength of novel corn stalk recombinant glulam component. Dynamic Systems and Applications 29(6): 20202969.
22. Tu, P.T., 2004: Building board produced by agricultural residues and its development status. Brick-Tile 12: 30-36.
23. Wang, J., Duan, S., He, J., Wang, Z., 2019: Experimental analysis of eccentric compression performance of larch wood-steel composite columns. Advances in Civil Engineering 2019: 1-17.
24. Wechsler, A., Hiziroglu, S., 2007: Some of the properties of wood-plastic composites. Building and Environment 42(7): 2637-2644.
25. Wei, Y., Zhou, M., Zhao, K., Zhao, K., Li, G., 2020: Stress-strain relationship model of glulam bamboo under axial loading. Advanced Composites Letters 29.10.1177/2633366X20958726.
26. Xie, Z., Hu, X., Du, H., Zhang, X., 2020: Vibration behavior of timber-concrete composite floors under human-induced excitation. Journal of Building Engineering 32: 101744.
27. Yang, R., Li, H., Lorenzo, R., Ashraf, M., Sun, Y., Yuan, Q., 2020: Mechanical behaviour of steel timber composite shear connections. Construction and Building Materials 258: 119605.
28. Zhang, X.B., Jiang, Z.H., Fei, B.H., Fang, C.H., Liu, H.R., 2020: Experimental performance of threaded steel glued into laminated bamboo. Construction and building materials 249: 118780.
29. Zhao, W., Yang, B., Zhou, J., 2019: Axial compressive creep behaviour of a square steel tube/bamboo plywood composite column with binding bars. Wood Research 64(2): 223-235.

XUE FENG, BOXIN WANG
JILIN UNIVERSITY
COLLEGE OF CONSTRUCTION ENGINEERING
CHANGCHUN, JILIN 130021
CHINA

YONGMEI QIAN*, WEI TIAN
JILIN JIANZHU UNIVERSITY
CHANGCHUN, JILIN 130118
CHINA
*Corresponding author: qianyongmei@jlju.edu.cn